THE JOURNAL OF PHYSICAL CHEMISTRY C
A JOURNAL OF THE AMERICAN CHEMICAL SOCIETY

pubs.acs.org/JPCC
Article

Acidity and Phase Behavior of Frozen Hydrochloric Acid during Thawing

Published as part of The Journal of Physical Chemistry C special issue "Heterogeneous Drivers of Ice Formation".

Radim Štůsek, Lukáš Veselý, Markéta Melicharová, Jan Zezula, Johannes Giebelmann, Thomas Loerting, and Dominik Heger*

Cite This: *J. Phys. Chem. C* 2024, 128, 17674–17685

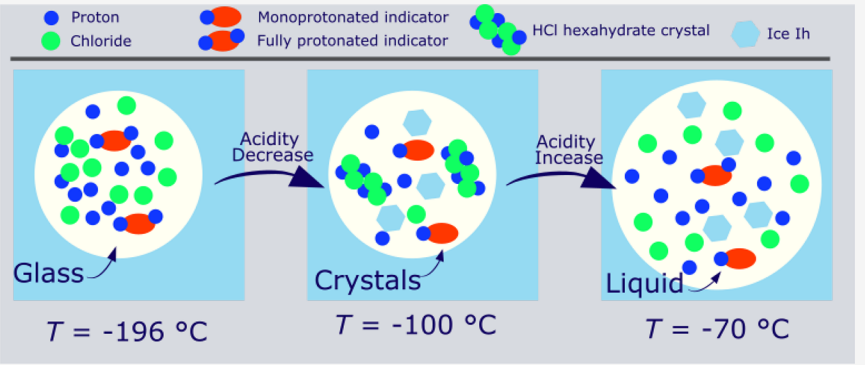

ABSTRACT: Freezing and its application is growing in popularity, yet the understanding of the nonequilibrium transformations and acidity changes that occur in frozen solutions upon thawing have remained relatively unexplored. By contrast to other acids such as nitric acid and sulfuric acid, not even the phase diagram is known fully for hydrochloric acid. Even more importantly, the nonequilibrium transformations upon heating glassy freeze-concentrated solution (FCS) are also not well understood and freeze concentration lacks quantification. This work rectifies the knowledge gap by providing the freeze-concentration factors on the example of hydrochloric acid. For this purpose, we have used differential scanning calorimetry to reveal phase changes upon heating. UV−vis spectroscopy of acid−base indicators is employed to elucidate acidity changes. All the samples reach negative values of the Hammett acidity function from −2.5 to −0.25 after freezing, showing that aqueous HCl can freeze concentrate 7−250,000 times depending on its initial concentration. We observe the glass-to-liquid transition of the freeze-concentrated glassy solution above −140 °C and cold crystallization of the ultraviscous FCS to HCl hydrates above −110 °C. Cold crystallization leads to basification, whereas acidification accompanies the subsequent melting of the eutectic ice/HCl-hexahydrate. Finally, melting of the ice immersed in solution shows basification caused by the dilution with meltwater. High (1 M) and low (<10 mM) concentrations freeze homogeneously, whereas intermediate concentrations reveal the presence of freeze-concentrated regions of higher and lower concentrations having distinct glass transition and melting temperatures.

INTRODUCTION

Hydrochloric acid or aqueous hydrogen chloride is one of the most common strong inorganic acids. It is omnipresent, from the human stomach[1] to the atmosphere[2] and beyond in the cosmic dust.[3,4] In astrochemistry, HCl-ice is the main reservoir of chlorine in protostellar conditions.[3,5] The adsorption of HCl on ice has been described in the Martian atmosphere,[6] where it undergoes interesting photochemical transformations.[7]

In Earth's stratosphere, HCl in trace amounts is capable of melting the surface of ice crystals at −90 °C, thereby producing a liquid layer on the surface of polar stratospheric ice cloud particles.[8] The liquid layer at −90 °C is highly reactive and converts chlorine reservoir species (such as HCl itself and chlorine nitrate) to active chlorine species during the polar winter. These active chlorine species are responsible for the formation of the springtime polar ozone hole during the polar sunrise.[9,10] In the troposphere of Earth, the data are even more numerous, as it is presumed that HCl is one of the main sources of acidity of naturally occurring aerosol particles.[11,12] Its penetration into the ice particles has been studied

Received: July 7, 2024
Revised: September 20, 2024
Accepted: September 25, 2024
Published: October 3, 2024

https://doi.org/10.1021/acs.jpcc.4c04540
J. Phys. Chem. C 2024, 128, 17674−17685

thoroughly,[13] since the chlorides are known to incorporate into the pure ice crystals during freezing, which charges the ice−solution interface. The effect was described by Workman and Reynolds and thus bears their name.[14] The charged interface is unstable, and at some point, the charge induced by the chlorides is neutralized by a counterion, which is usually a proton or a hydroxyl since they are the most mobile ions. This, of course, deprives the remaining solution of these ions, either basifying them (if protons are incorporated) or acidifying them.[15−17] The thermal properties of HCl solutions were examined in bulk[18] and in nanoscale.[19,20] Previously, HCl freeze-concentrated in the glaciers has been found to associate with volcanic events and forest fires.[21] After incorporation into the ice, the chloride produces point defects in the ice crystal, namely, charged defects and Bjerrum-L-defects. Such defects play a key role for electrical conduction in ice[22] and for the rate of water dipole reorientation in the ice lattice, producing H-ordered ice at low temperatures.[23,24] The freezing of HCl solution leads to the enhancement of the cresol red protonation.[16]

The phenomenon of freeze concentration has been the subject of considerable research.[25−28] As a solution containing some amount of solutes begins to freeze, the water from the solution gathers into the ice crystals, thereby concentrating the solutes into a freeze-concentrated solution (FCS).[29,30] This process results in the formation of a composite solid−liquid material with quite a complex structure, often denoted as an ice matrix. Previous studies of freeze concentration of methylene blue, used as a probe molecule, demonstrated that the solute itself is capable of concentrating by a factor of 10^3-10^6 within the ice matrix.[31] Sulfuric acid of a concentration of 1 M has been detected in the veins of glaciers;[32] the later studies revealed somehow lower typical concentrations for sulfuric (c = 3.42−14.35 μM) and nitric acid (c = 1.48−6.57 μM).[33] Antarctic ice is highly conductive and shows huge creep because sulfuric acid accumulates at junctions between ice crystals, especially triple junctions.[34] By contrast, Greenland ice is not acidic, is not conductive, and barely shows any creep—the acid has been neutralized by basic dust there.[35] The complexity of the ice matrix is further emphasized by the heterogeneity of the sample; the vein diameters decrease with diminishing the initial concentration of solution and freezing rates.[30,36] The process of freeze concentration has been recognized to occur at two different levels, namely, the micro- and macro-freeze concentration.[37] The former results in FCSs trapped between the finer structures of ice crystals such as small needles, ferns, or dendrites.[38] The latter is caused by the pushing of the solution due to a broad, growing ice front. Those two processes lead to FCSs of two different concentrations, highly freeze-concentrated FCS_1 and, in comparison, the less concentrated FCS_2. Technologically, the process of freezing is employed to desalinate seawater[39] and concentrate food products.[40,41] Furthermore, the freeze concentration of mixtures with NaCl has been used to enhance the analytical signal by several orders of magnitude.[42]

Upon cooling, the solutes in the FCS may follow either the kinetic or thermodynamical pathway. By the former, the FCS transforms into amorphous quenched material or glass in a process known as vitrification. That is, the FCS may persist metastably upon continued cooling and finally vitrify to a glassy state. While persisting metastably, the concentration of the FCS increases further and further and can exceed the concentration given by the solubility limit in the stable phase. At the glass transition, the freeze concentration is concluded and the maximally FCS is reached.[43−45] In contrast, the latter thermodynamic pathway necessitates the crystallization of the eutectics. Previous studies have shown that HCl tends to form glassy material upon relatively fast cooling.[18−20] Compared to the well-known nitric[46] and sulfuric acid[47] eutectics that are in great agreement with computed data,[48] there is surprisingly no agreement in the eutectic temperature and composition for the HCl-H_2O system. The concentrations of the eutectic as hydrochloric acid hexahydrate ($HCl \cdot 6H_2O$) have been estimated to be 7.62 M[49] and 7.31−7.70 M.[50] The position of the eutectic having the composition corresponding to the hexahydrate is complicated by the proximity of the second eutectic with the composition of the trihydrate ($HCl \cdot 3H_2O$). A theoretical study, focusing on the strong acid chemistry under low temperatures, estimates the eutectic to be at 6.61 M.[48] The variety of these values shows that the behavior of HCl during freezing remains ambiguous and needs to be studied further.

Our method used for the determination of the acidity of FCS is UV−vis based. It consists of addition of a small amount of spectroscopically active acid−base indicator into the aqueous HCl solution and freezing of the sample. The measurement of the frozen sample is complicated by the light scattering of the polycrystalline ice sample, which we compensate by using an integrating sphere able to collect scattered light. This method has been successfully utilized to probe the acidity of frozen sodium phosphate solution,[51] NaCl solutions,[15] and solutions of pharmaceutically relevant buffer systems.[52,53]

This article focuses on the freeze concentration of HCl into a freeze-concentrated solution distributed between the ice crystals during freezing and subsequent warming by means of UV−vis spectroscopy. To determine the behavior of HCl within the unfrozen veins, we coupled our results with differential scanning calorimetry to connect the trends in acidity to the thermally induced phase behavior.

METHODS

Freezing, UV−Vis Measurement, and Data Treatment. The samples in poly(methyl methacrylate) UV−vis cuvettes (base 1 × 1 cm) with a total volume of approximately 3−4 mL were cooled in liquid nitrogen (T = −196 °C) at a rate of approximately 300 K/min[54] and cold-loaded into the Agilent Cary 5000 spectrophotometer. The temperature during heating in ambient air was measured, where the heating rate was not kept constant. The spectrophotometer is equipped with an Agilent Internal DRA-2500 Integrating sphere, the purpose of which is to collect all the scattered light from the polycrystalline ice sample.

Frozen pure water's spectrum was used as a baseline and was thus subtracted from each sample. The spectra of pure forms of the indicator−the acidic and basic forms (A and B, respectively) were obtained from titration.

The spectra of each sample at each temperature were then fitted with the spectra of pure forms via a MATLAB routine by a least-squares non-negative algorithm (function lsqnonneg). The relative abundancy of each form in the sample was obtained by this procedure, and they were further used to calculate the Hammett acidity function.

Hammett Acidity Function. The Hammett acidity function was developed to probe highly acidic media and solid acids; it is thus ideal for the purposes of this work. The

https://doi.org/10.1021/acs.jpcc.4c04540
J. Phys. Chem. C 2024, 128, 17674−17685

Table 1. Values of Coefficients k_1−k_6 Used for the Calculation of Hammett Acidity Function and Concentration of HCl with a Known Weight Percentage of the Acid

coefficient	k_1 /%$^{-1}$	k_2 /%$^{-2}$	k_3 /%$^{-3}$	k_4 /%$^{-4}$	k_5 /%$^{-5}$	k_6 /%$^{-6}$
values for H_0	-4.164×10^{-2}	-1.184×10^{-3}	-5.720×10^{-5}	5.681×10^{-6}	-1.932×10^{-7}	2.192×10^{-9}
values for c	2.737×10^{-1}	1.274×10^{-3}	7.214×10^{-6}	-4.472×10^{-7}	1.877×10^{-8}	-2.907×10^{-10}

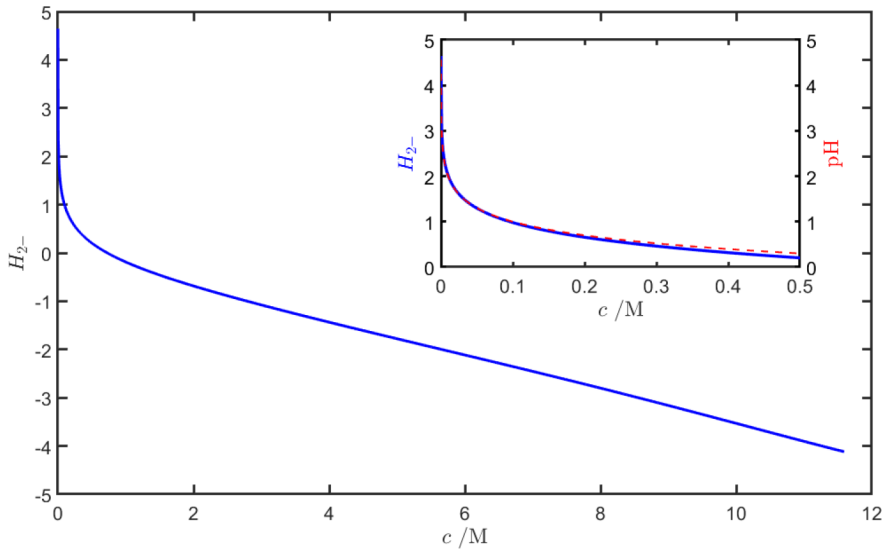

Figure 1. Dependence of Hammett acidity of HCl on its concentration. The inset plot shows how the Hammett acidity (in blue) compares to the pH (dashed line in red) in the relevant range from 0 to 0.5 M acid concentrations. Data for the plot was taken from Kresge et al.[59]

simple equation of Hammett acidity originates from the acid−base equilibria of an indicator:

$$H_nA \leftrightarrow H^+ + H_{n-1}A^-$$

The dissociation constant from the equilibrium is constructed and yields

$$K_a = a_{H^+} \times \frac{a_{H_{n-1}A^-}}{a_{H_nA}}$$

Rearrangement and application of a negative decadic logarithm yield the Hammett acidity function for a general n-protic acid:

$$H_{n-} = pK_a + \log_{10}\left(\frac{a_{H_{n-1}A^-}}{a_{H_nA}}\right)$$

In the equation, pK_a and activities are dependent on the chemical environment, mainly ionic strength and temperature. First, the dependence on temperature for the sulfonephthalein indicators is quite weak. In the case of BCP in the temperature range of 10−30 °C, pK_{a2} shows a negative association; it decreases by about 0.1 units on this interval.[55] On the other hand, pK_a generally shows a negative association with ionic strength up to a certain value, above which, however, pK_a shows a positive association instead.[56−58]

The exact value depends on the compound and the chemical environment. In the case of BCP, pK_{a2} drops to about 6.10 at moderate ionic strength and subsequently rises at higher ionic strengths, reaching values higher than those of pK_a in dilute solution. This dependence was not studied for pK_{a1}; however, we have performed titrations of the indicator in concentrated hydrochloric acid. Thus, this dependence should be eliminated if the samples of relatively high concentrations of HCl are measured.

Concentration Factor. The concentration factor is used as a measure of freeze concentration. It is defined, for the purposes of this work, as the ratio of HCl in the FCS and the initial HCl concentration:

$$f_c = \frac{c_{frozen}}{c_{initial}}$$

The initial concentration of HCl ($c_{initial}$) was calculated from dilution of the stock solution. The concentration of HCl after freezing of ice (c_{frozen}) was calculated from the available data in the work, the Hammett acidity function values. We emphasize that the concentration of HCl represents an average over all noncrystalline regions in the sample, which includes the FCS located in the veins (which are a result of macroscopic cryoconcentration) but also the trapped FCS that is located in between small features of the ice crystals caused by the microscopic cryoconcentration. Kresge et al.[59] measured the acidity function of HCl and its dependence on the weight percent (w) of HCl, as well as the concentration weight percent dependence on concentration of the acid. The work provides the following pseudopolynomial expression for the calculation of Hammett acidity (H_0) and concentration depending on the weight percent w:

$$H_0 = -0.4450 \times \ln w + 0.5474 + k_1 w + k_2 w^2 + k_3 w^3 + k_4 w^4 + k_5 w^5 + k_6 w^6$$

$$c = k_1 w + k_2 w^2 + k_3 w^3 + k_4 w^4 + k_5 w^5 + k_6 w^6$$

The expression was used to calculate the acidity function of HCl (values of coefficients k_1−k_6 are given in Table 1).

https://doi.org/10.1021/acs.jpcc.4c04540
J. Phys. Chem. C 2024, 128, 17674−17685

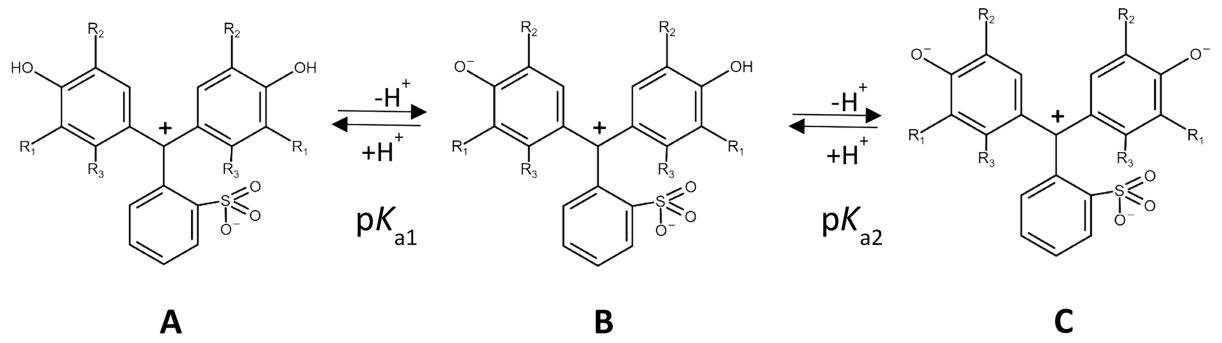

Figure 2. First-order dissociation (A−B equilibrium) and second-order dissociation (B−C equilibrium) for a general structure of sulfonftalein indicator. In the case of CPR, the substituents are R1 = Cl, R2 = H, and R3 = H; in the case of BCP, the substituents are R1 = Br, R2 = CH_3, and R3 = H.

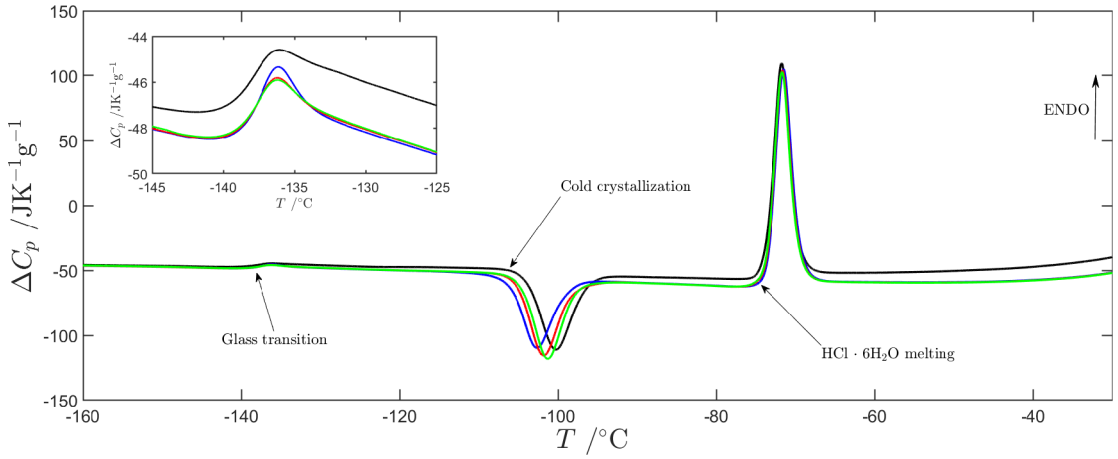

Figure 3. A thermogram of 1 M HCl in the relevant temperature range of −160−30 °C; the black line signifies cold-loaded sample (frozen outside the DSC in liquid nitrogen). The blue, green, and red lines show heating scans (30 °C/min) of samples cooled by the rate of 30 °C/min. The inset plot shows a magnification of the glass transition in the relevant range of −145 and −125 °C.

The dependence of Hammett acidity on the concentration of HCl is shown in Figure 1 with dedicated comparison of the Hammett acidity to the commonly used pH scale, which is visible in the inset of Figure 1. The Hammett acidity reaches a unity with the pH scale below a concentration of 0.1 M (pH 1). Above this point, the use of Hammett acidity is necessary for correct determination of acidity and thus concentration of the acid.

The calculation of concentration from a known value of Hammett acidity was performed by a spline embedded in a MATLAB routine (Script S1), which takes in a vector of Hammett acidities and returns a vector of concentrations along with a plot showing this dependence and the splined points.

Titrations of the Acid−Base Indicators. The indicators bromocresol purple (BCP) and chlorophenol red (CPR) were titrated in HCl to obtain the first-degree dissociation constant (pK_{a1}). Each indicator is diprotic; each of them possesses three spectral forms, the most acidic A-form, the neutral B-form, and the basic C-form. Their equilibria are shown in Figure 2. Titration was performed by preparing solutions of indicators in concentrated HCl and titrating the solution with water. A selected experimental run for BCP is depicted in Figure S1A and that for CPR in Figure S1B.

Spectra of pure forms of the BCP and CPR were measured (Figure S2A and B, respectively), and the titration was treated by a SpecFit routine, which yielded the pK_{a1} values. The pK_a values were calculated from these experiments, and the resulting pK_{a1} values were −1.922 ± 0.002 (2) and −1.475 ± 0.028 (2) for BCP and CPR, respectively.

Differential Scanning Calorimetry Measurements. The solutions of HCl with concentrations of 1 M (3.59%$_w$), 100 mM (0.365%$_w$), 10 mM (0.037%$_w$), and 1 mM (0.0037%$_w$) were prepared. 10 μg of them was transferred to aluminum pans, which were subsequently hermetically sealed at room temperature, frozen in liquid nitrogen, and quickly loaded into the DSC (PerkinElmer DSC8000) at −180 °C, a procedure known as a cold-loading, which was developed and used frequently over the past decades in the Loerting lab (e.g., refs 60,61). In the DSC instrument, the samples were heated to the temperature of 50 °C by a rate of 30 °C·min^{-1}, and subsequently three cycles of cooling (30 °C·min^{-1}) to −180 °C and heating (30 °C·min^{-1}) to 50 °C were performed.

The baseline (i.e., the trace of pure hexagonal ice) was subtracted from the resulting thermograms, and further analysis was performed in Origin software. Also, this procedure has been used for decades in the Loerting lab.

RESULTS AND DISCUSSION

Calorimetric Measurements of HCl. The sample of 1 M HCl (Figure 3) shows several reproducible features in the heating thermogram: first, the glass transition that occurs at $T_g \approx -138$ °C, second, the cold crystallization at $T_c \approx -110$ °C, and, third, the melting of ice/hydrochloric acid hexahydrate at $T_m \approx -75$ °C. Above this temperature, a slight rise in thermal

https://doi.org/10.1021/acs.jpcc.4c04540
J. Phys. Chem. C 2024, 128, 17674−17685

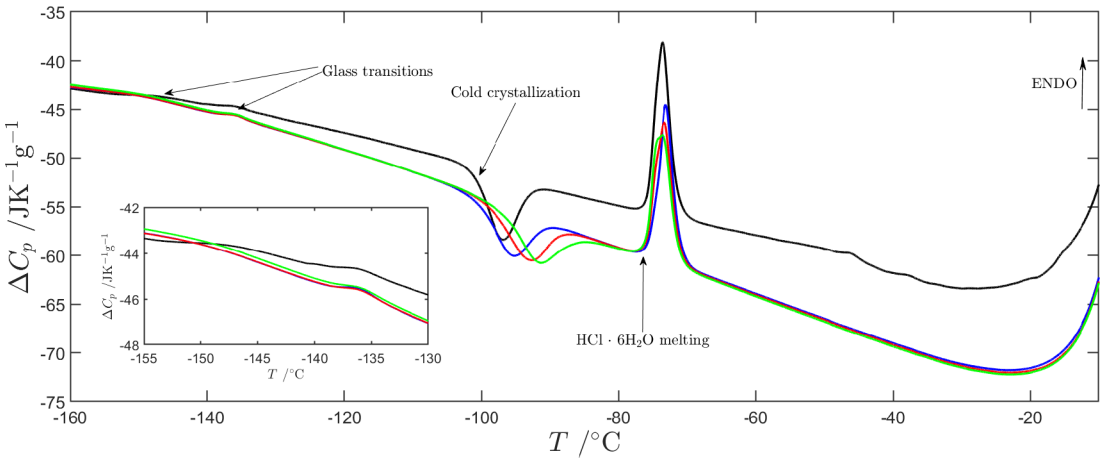

Figure 4. A thermogram of 100 mM HCl in the temperature range of −160 to −10 °C, the black line signifies cold-loaded sample (frozen outside the DSC in liquid nitrogen). The blue, green, and red lines show heating scans (30 °C/min) of samples cooled by the rate of 30 °C/min. The inset plot shows a magnification of the glass transition in the relevant range of −155 and −130 °C.

capacity is noticeable, which shows the slow melting of ice immersed in HCl solution as the liquidus curve is followed until the complete melting of ice having a peak center at T = −1.10 °C. The full thermogram of the 1 M HCl sample is shown in Figure S3.

At this point, we deem it advantageous for the sake of clarity to redefine the symbols for the microscopic (FCS_1) and macroscopic (FCS_2) FCSs. The FCS_1 will hereby be denoted as FCS_H, the index of which signifies that it is of *higher* concentration than FCS_2, denoted further on as FCS_L for its *lower* concentration in comparison. The same argument applies for the notation of the glass transition temperatures (T_gs) as well. The Gordon−Taylor[54] equation predicts that the T_g of binary aqueous solution of higher concentration occurs at a higher temperature; thus, the $T_{g,1}$ will be denoted as $T_{g,H}$ and $T_{g,2}$ as $T_{g,L}$.

The melting temperature at $T_m \approx -75$ °C was previously assigned to the melting of HCl · $6H_2O$ in a calorimetric study of HCl.[18] Bogdan and Loerting[20] found two eutectic melting events at $T_m \approx -73$ °C for HCl · $6H_2O$ and $T_m \approx -87$ °C for HCl · $3H_2O$ in emulsified solutions of 17%$_{wt}$ HCl. For 20%$_{wt}$ solutions, only the ice/hexahydrate melting was observed, and for 21.5%$_{wt}$, no eutectic melting was observed, but merely a glass transition.[20] The glass transition has been documented to occur at the approximate temperature of −138 °C (135 K)[18] in the bulk ice samples with the heating rate of 4 °C·min^{-1}. Bogdan and Loerting[20] reported a glass transition temperature of −146 °C (127 K) for heating at a rate of 5 °C·min^{-1} in the calorimeter. The transition is located about 8 °C lower than that observed here (see inset of Figure 3), which is expected as the glass transition temperature shifts to lower temperatures with decreasing heating rates. The crystalline phases produced during the cold crystallization are unknown in the first place. However, based on the calorimetric data, it would appear that the trihydrate is absent (no trihydrate melting endotherm is observed), but the hexahydrate remains the only observed phase, as evidenced by the presence of a substantial endotherm of ice/hexahydrate melting.

The thermograms of 100 mM HCl (Figure 4) show the same major features as those of the sample of 1 M HCl: The glass transition occurs at ≈ −138 °C, while the cold crystallization and melting of the ice/HCl-hexahydrate eutectic occur at ≈−110 and ≈−75 °C, respectively. This means that supercooled liquid FCS of ultrahigh viscosity is present in the ice matrix from −138 to −110 °C, while between −110 and −75 °C, the FCS occurs as crystalline hydrate(s) and melts again at −75 °C. The heat taken up at the melting is smaller in this case (the ratio between 1 and 100 mM is 9.463 ± 0.018), reflecting that proportionately less ice/hexahydrate melts in this case. Interestingly, there is a second glass transition located near −150 °C (123 K) for the first heating scan (after rapid cooling of the sample in liquid nitrogen). We speculate that this could be the glass transition pertaining to a second FCS that is of lower concentration $T_{g,L}$. The second type of FCS (FCS_L) is no longer evident for the second and third heating scans, following a slower cooling of the sample at 30 K/min. Thus, it seems that the separation of FCS into its microscopic and macroscopic variants, FCS_H and FCS_L, respectively, is more pronounced for rapid cooling.

The fast cooling forms thinner veins where kinetically trapped FCS_H remains incarcerated and larger veins are filled by FCS_L; the situation is different on slow cooling, which results in a smaller number of thinner veins and all spaces are filled with the homogeneous FCS_H. Previously, a second glass transition in frozen 17%$_{wt}$ HCl was also observed by Bogdan and Loerting[20] in emulsified 5 μm droplets, but its nature has remained unclear (see Figure 3, magnified top trace in ref 20). Furthermore, the cold-loaded sample shows signs of several weak features located at roughly −50 and −40 °C. These peaks are either melting or crystallization, which is difficult to estimate given their shapes and intensities. This might again be a result of the FCS separation into FCS_L and FCS_H. The sample of 10 mM HCl (Figure S4) shows very small features; nonetheless, the position of the glass transition can be estimated to be roughly −145 °C, closer to the low freeze-concentrated case, although the precise position is difficult to assign. The cold crystallization cannot be observed. However, the cold-loaded sample shows a slight endothermic peak at ≈−35 °C, which is located well above the eutectic temperature. A fivefold increase in the sample mass for the calorimetric analysis gives rise to observable glass transition (T_g is shifted to approximately −145 °C), cold crystallization, and HCl · $6H_2O$ melting (Figure S5); even though the signal intensities are low, these features are clearly distinguishable from the noise.

https://doi.org/10.1021/acs.jpcc.4c04540
J. Phys. Chem. C 2024, 128, 17674−17685

In the following section, the detailed analyses of DSCs, beyond the abovementioned main thermal signatures, will reveal several interesting features. At first, the focus will be given to the region above the eutectic crystallization of $HCl·6H_2O$ (T = <−65 °C, −20 °C>), which will point to heterogeneity of the sample. The hypothesis of heterogeneity will be confirmed on the behavior of glass transitions (T_gs = −145 °C, −138 °C). These findings are schematically summarized in the combined phase-state diagram in Figure S14.

A straight line, correcting the baseline drift, was subtracted from the thermograms of the cold-loaded 1, 100, and 10 mM HCl samples to enhance the visibility of the peaks within the range of −65 to −30 °C (Figure S6). The sample of 1 M HCl shows two small peaks located at −63 and −61 °C, while the 100 mM HCl sample shows a great number of peaks, the most notable ones being located at temperatures of −47 and −38 °C (based on the peak maxima), whereas the thermogram of the 10 mM sample shows only one significant peak having maximum at the temperature of −34 °C and a shoulder at −38 °C. The first derivative of each cold-loaded sample is depicted in Figure S7 and shows the discussed features more clearly, mainly two small peaks located at −63 and −61 °C in the thermogram of the 1 M HCl sample. On the other hand, numerous features can be observed in the 100 mM HCl thermogram, the most significant being the mentioned peaks at −47 and −38 °C, along with a large number of peaks of low intensity. The 10 mM sample remains almost featureless up to the temperature of −40 °C, whereby the derivative shows several peaks superimposed on the main peak with maximum of −34 °C.

The first derivative of heat capacity with respect to temperature in the range of −65 to −30 °C (Figure S7) shows, most importantly, the shift of peak maxima to higher temperatures with decreasing initial HCl concentration. The nature of the peaks is unknown; we hypothesize that they correspond to either unstable higher HCl hydrates or HCl solutions, of lower than eutectic composition, either crystallized or vitrified. This implies that the sample would have to be quite heterogeneous, composed of the regions (possibly in between ice dendrites) containing $HCl·6H_2O$ and the other regions (possibly veins) containing HCl surrounded by a larger amount of water molecules, giving rise to the peaks at T >−65 °C. The peaks at lower temperatures (around −60 °C), as is the case for 1 M HCl sample, would correspond to a relatively higher acid concentration than the ones at a higher temperature (around −35 °C), as is the case for the 10 mM HCl sample. If recalculated to concentrations of HCl from the phase diagram,[48] the concentrations would be roughly 5.7 and 4.1 M for the melting temperatures of −60 and −35 °C, respectively. This difference of concentration is quite typical for the two different processes of micro- and macro-freeze concentrations. Typically, the cryoconcentration at the microscale leads to more concentrated FCS_H compared to FCS_L produced at the macroscale inside the veins or at the frontier of the growing ice front. This was nicely shown, for instance, on the example of citric acid using a combination of optical cryomicroscopy and calorimetry.[38] That is, in the present case, the less concentrated 5.7 and 4.1 M solution would be located in the veins between ice crystallites, whereas the eutectic hexahydrate composition near 7 M is found around the microscopic dendrites, which form, most likely, the structures inside the veins (as can be seen on the Figure 3B in Veselý et al.[36]).

The subsequent analysis was conducted in the low-temperature region (below —130 °C), where a glass transition was observed. A detailed examination of the regions reveals the presence of two potential glass transitions. These two glass transitions for HCl were previously identified by Bogdan and Loerting.[20] In their work, they identified T_{g1} as the glass transition of an FCS with a higher concentration of HCl, which they designated as FCS_1 ($T_{g,H}$ and FCS_H in the present work). $T_{g,2}$ on the other hand, was identified as the glass transition of an FCS with less concentrated HCl, which they designated as FCS_2 ($T_{g,L}$ and FCS_L). The glass transition observed in our experiments, occurring at −138 °C ($T_{g,H}$), is dominant at a high concentration (1 M HCl). Conversely, the subsequent transition at −150 °C ($T_{g,L}$) is relatively minor at this concentration (approximately 6%, based on the change in thermal capacity before and after each transition), as illustrated by the first derivative in Figure S8. The ratio between $T_{g,H}$ and $T_{g,L}$ is decreasing with a decreasing concentration of HCl; for the 10 mM sample, $T_{g,L}$ remains the only observable glass transition (Figures S4 and S5). The major glass transitions visible in the thermograms of 1 M and 100 mM samples both occurred at the same temperature of −138 °C ($T_{g,H}$), albeit the glass transition in 100 mM ($T_{g,H}$ = −138 °C) shows some additional superimposed feature. The fact that the second glass transition's ($T_{g,L} \approx$ —145 °C) relative intensity to $T_{g,H}$ visibly increases with decreasing concentration further emphasizes our hypothesis of heterogeneity. In this context, it needs to be noted that T_g typically decreases with decreasing concentration, reaching minimum at concentrations <4%$_{wt}$, subsequently rising to that of the pure solvent.[62] To reiterate, $T_{g,H}$ is associated with the FCS_H of higher concentration that is produced by microfreeze concentration. In turn, this means that for 1 M, HCl concentrates mostly to FCS_H (possibly in the microscale), whereas for the 10 mM solution, the concentration at the macroscale is more important. At 100 mM the cooling rate determines which of the two processes contributes more. In nanoscale fumed silica, the $T_{g,2}$ for HCl has been reported to shift to slightly lower temperatures (−153 to −148 °C).[19] We can thus presume that the ice matrix is composed of both the veins with a "bulk" glass composition and the others having a glass of lower than eutectic composition.

Let us now roughly estimate the size of the liquid domains within the ice matrix. Assuming that the majority of the 10 mM sample has to concentrate to the eutectic composition (based on the presence of $HCl·6H_2O$ melting in Figure S5 and Table S1), we can determine the theoretical concentration factor to be about 700 (based on the values of c_e = 7 M, c_i = 0.01 M). The DSC experiments were conducted with a 10 μL sample; the resulting volume of FCS would thus be 14 nL. It is thus quite possible that if the FCS is separated into several 10−100 of veins, each vein with a volume of fraction of a nanoliter can act as a compartment small enough for the effects comparable to those observed by Bogdan et al.[19] to take place. On the other hand, samples of larger initial concentrations show intense $T_{g,H}$ and a slight presence of $T_{g,L}$; thus, they form a more homogeneous system, with 10 and 100 times higher FCS volumes for the samples of 100 mM and 1 M HCl, respectively.

The calorimetry of HCl solutions of similar concentrations as in this work has been measured on porous silica, which

https://doi.org/10.1021/acs.jpcc.4c04540
J. Phys. Chem. C 2024, 128, 17674−17685

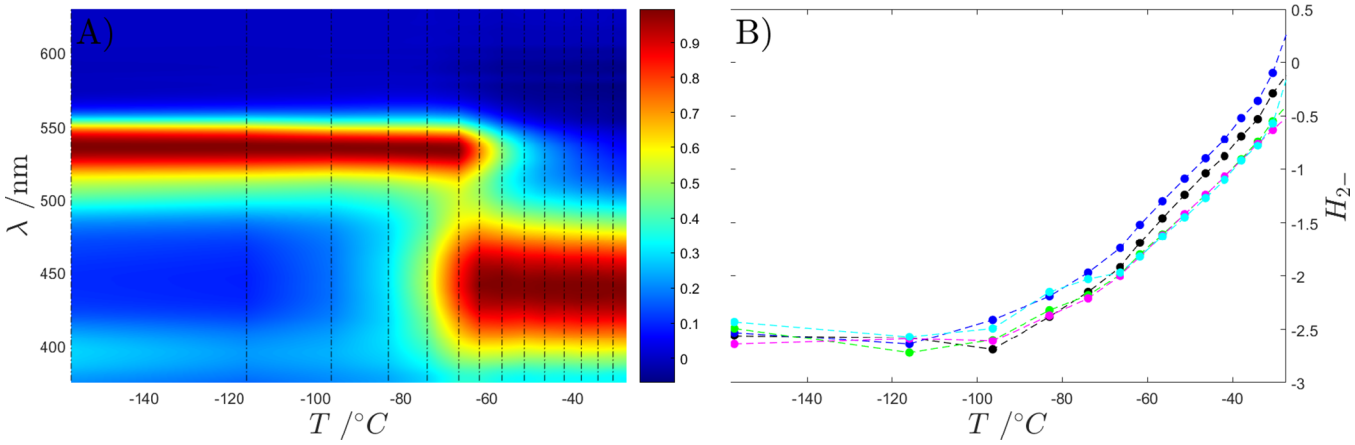

Figure 5. (A) Dependence of averaged normalized BCP spectra on temperature for 1 M HCl left to heat from −196 °C to room temperature. The color bar shows the normalized absorption of the spectra. (B) Dependence of Hammett acidity of 1 M HCl frozen solution; each run of the experiment is plotted in different colors.

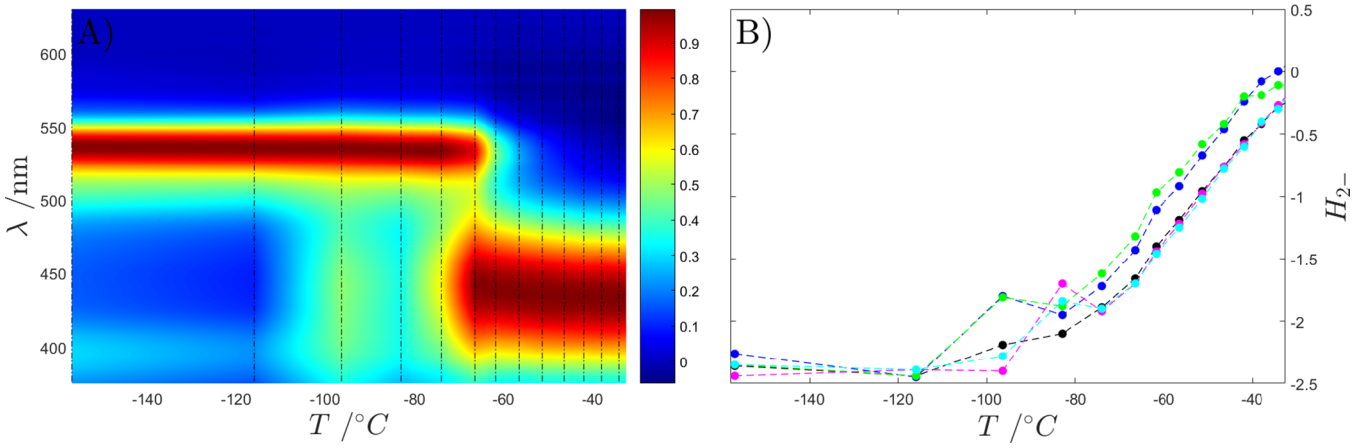

Figure 6. (A) Dependence of selected BCP spectra on temperature for 100 mM HCl left to heat up from −196 °C to room temperature. The color bar shows the normalized absorption of the spectra. Spectra are not averaged, because the average does not sufficiently depict the sudden rise in basicity. (B) Dependence of Hammett acidity of 100 mM HCl frozen solution; each run of the experiment is plotted in different colors.

showed a significant increase in melting temperature up to −40 °C due to the adsorption of the acid droplets on the water−silica interface.[19] Similar experiments were performed for HCl with high initial weight percentage (54−1.4%$_w$).[19] The highest HCl concentration probed in the mentioned work (54 ± 10%$_w$) showed melting at −40 °C, which the authors assumed to correspond to a different hydrate formed by the unique environment of the silica. In our work, we do not know the precise identity of the phases either. However, the spread of crystallization temperatures (from −65 to −30 °C, Figures S6 and S7) points again to the fact that the sample is not homogeneous. Because the features are detectable only in the cold-loaded sample, their presence is induced by fast cooling rates, which leads us to interpret the melting peaks at temperatures higher than −75 °C to correspond to the quenched HCl solutions with concentrations lower than the eutectic one.

Acidity of Frozen HCl Solutions and Its Melting. The HCl solutions were prepared by dilution of the HCl stock solution (c = 2.00 M). The probed concentrations ranged from 1 M down to 5 μM; acid−base indicator BCP ($c = 7 \times 10^{-6}$ M) or CPR ($c = 9 \times 10^{-6}$ M) was added to the solutions, and these were frozen in liquid nitrogen. Subsequently, the frozen solutions were left to warm up at room temperature in the spectrophotometer, and their spectra and temperature were recorded simultaneously (Figures 5A and 6A and Figures S9A−S12A).

The absorption spectra of the acid−base indicators were utilized in calculating the H_{2-} values (see Methods), and both are plotted in Figures 5B and 6B and Figures 9B−S12B. Each spectrum was measured for 30 s; the indicated temperature is the middle of the temperature interval (between 0 and 30 s, the temperature recorded at 15 s is shown). Because of this technical arrangement, the temperature rises rapidly in the beginning and rather slowly at the end of the melting experiments, and thus, the temperature intervals are unevenly distributed. Nevertheless, the lower and upper bounds of each interval are given in Table S2 along with the corresponding H_{2-} values.

The heating of 1 M HCl solution from −196 °C (Figure 5A) shows no significant shifts in acidity changes up to the temperature of −100 °C, at which the gradual decrease in acidity starts. There are only slight changes at the beginning of heating (−160 to −120 °C), which could be attributed to a glass-to-liquid transition occurring at an onset temperature of ≈−138 °C (compare with thermogram in Figure 3). Above −85 °C, the acidity gradually decreases, which can be attributed to the dilution of HCl inside the veins by the ice

https://doi.org/10.1021/acs.jpcc.4c04540
J. Phys. Chem. C 2024, 128, 17674−17685

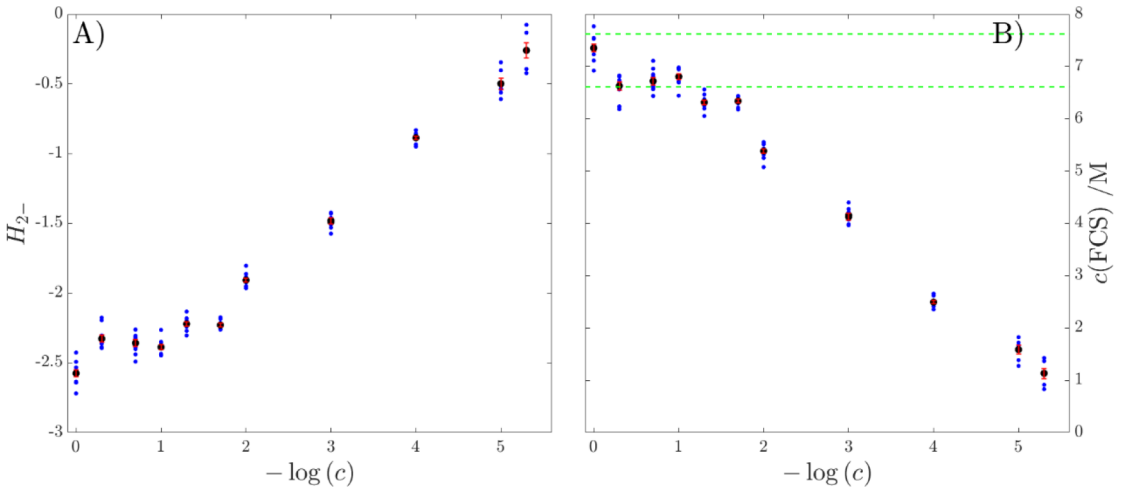

Figure 7. (A) Hammett acidity dependence on the negative decadic logarithm of initial concentration of HCl in the temperature range of −196 to −120 °C is shown as blue points; the averaged Hammett acidities (black) are depicted with error bars showing the standard error of the mean (red). (B) Dependence of the HCl concentration in FCS depicted on the negative decadic logarithm of the initial HCl concentration as blue points with the average concentration (black) and error bars showing the standard error of the mean (red). The green lines show the upper and lower boundaries for the HCl eutectic. The recalculation from H_{2-} to concentration was performed by the pseudopolynomial given in Kresge et al.[59]

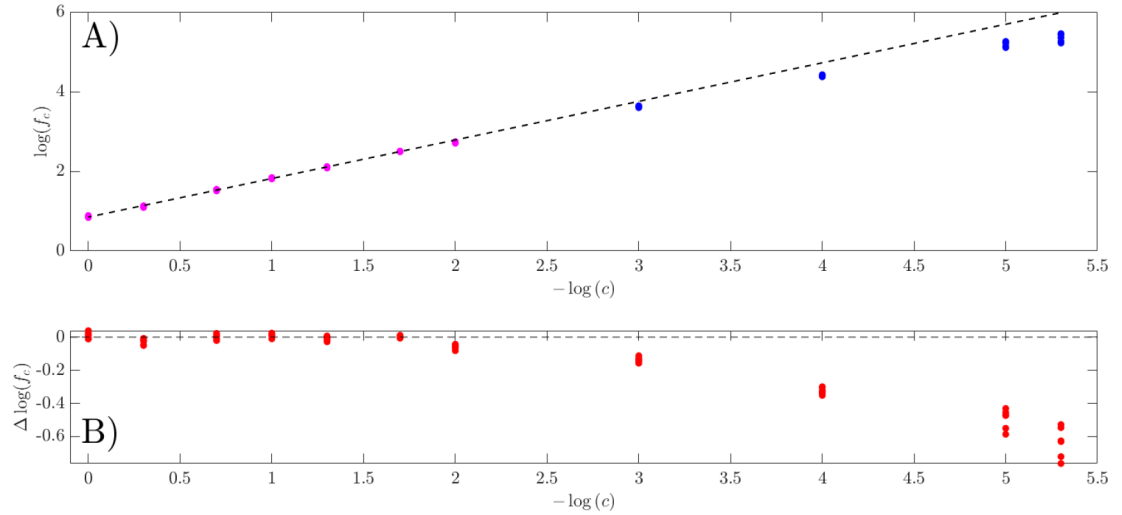

Figure 8. (A) Dependence of concentration factor f_c on the initial HCl concentration in a double logarithmic plot. The magenta points show samples measured with BCP, whereas the blue points show samples measured with CPR (at −log(c) = 3 both CPR and BCP points are present; they however overlap). The black line shows a linear fit up to a concentration of 20 mM (−log(c) = 1.69). (B) Difference of the fitted line and the calculated f_c depicted in red with zero line shown in black. The data with averages and their SEM values are given in Table S3.

melting. Averaging the first two points (T = −150 and −115 °C) in each repeated measurement yields a H_{2-} = −2.57 ± 0.03, corresponding to a concentration of c_{frozen} = (7.34 ± 0.08) M; the concentration factor calculated from this concentration is then f_c = 7.34 ± 0.08.

On the other hand, 500 mM HCl (Figure S9) shows a repeatable spike in Hammett acidity at −95 °C and an immediate increase in acidity at −85 °C, where subsequently the acidity gradually decreases. This trend is followed in the samples of 200 mM HCl (Figure S10) and 100 mM HCl (Figure 6), where the spike of similar magnitude shifts in its central position to either −95 or −80 °C. Apart from this shift, which is most likely caused by the experimental setup allowing no temperature control, the spike is due to the decreases in acidity by cold crystallization, which is immediately followed by an acidity increase and a subsequent gradual acidity decrease. The spike can be recognized also in the 50 mM sample (Figure S11). However, they are no longer present in the 10 mM sample (Figure S12), which is similar to the 1 M sample in terms of acidity (Figure 5). Furthermore, the acidity at the lowest temperatures (−150 and −115 °C) increases as the initial concentration decreases.

The sudden decrease in acidity (basicity spike) can be attributed to cold crystallization of FCS to the HCl hexahydrate (with onset at approximately −110 °C). The cold crystallization at −110 °C siphons the protons and chloride ions from the FCS into the HCl·6H_2O crystals, making the resulting FCS less acidic. On the other hand, melting of the HCl·6H_2O crystals at −75 °C brings the protons back to the FCS again, causing acidification (Figures 6 and Figures S9−S11). We do not, however, know why the sudden change in acidity upon cold crystallization is observed in the samples of 500−50 mM concentrations but not

https://doi.org/10.1021/acs.jpcc.4c04540
J. Phys. Chem. C 2024, 128, 17674−17685

identified for solutions of both higher and lower concentrations.

Plotting the acidities of all the measured samples at −150 and −115 °C against the HCl concentration shows that with decreasing concentration, the Hammett acidity increases (Figure 7A), which means that the acidity of the sample decreases. Nonetheless, all observed values of the Hammett acidity function are below zero, which signify very acidic conditions. Recalculating the Hammett acidity to concentration (via Kresge's equation[59]) shows that the average concentration of HCl in the ice matrix decreases with initial concentration (Figure 7B). This observation agrees with the calorimetric data, which show that at lower concentrations, the sample is not able to fully freeze-concentrate to the eutectic $HCl{\cdot}6H_2O$; instead, it forms quenched HCl with concentrations lower than that of the eutectic (Figure S6). The effect is apparently stronger at lower initial concentrations. Interestingly, the indicator can probe this region of low concentrations, even though the thermal signatures in the DSC are too low to be observed for solutions having an initial concentration below 1 mM in HCl.

The 1 M sample reaches a concentration of HCl in the veins of 7.35 M. The eutectic concentration of HCl has been debated in the literature; a range of eutectic compositions exists, namely 24.8%, corresponding to 7.62 M[49] and 7.01 M.[48] However, computational studies suggest that by accounting the ion uptake into the ice, the hexahydrate eutectic should shift to 6.61 M. Even though the precise eutectic is not known, we have used the value of 7.62 M as upper boundary and the value of 6.61 M, recommended by ref 48, as a lower boundary; both are shown in Figure 7B as green dashed lines. The samples of higher concentration (1 M to 100 mM) fall within the eutectic boundary; based on this, we can estimate that the sample freeze-concentrated to the eutectic concentration. The samples of 50 and 20 mM HCl are quite close to this range, and for the purposes of further analysis, they will be considered also of eutectic composition.

The concentration factors were calculated from the data in Figure 7B. The concentrations of HCl in FCS were simply divided by the initial concentration, and the decadic logarithms of the factors are plotted on negative decadic logarithms of the HCl concentration in Figure 8A, and the concentration factors are shown also in Table S3.

The increase in concentration upon freezing in liquid nitrogen is only sevenfold in the case of 1 M HCl, and the factor steadily increases with decreasing concentration, reaching values of roughly 250,000 for 5 μM. This shows that for the less concentrated samples (5−100 μM), the increase in concentration can be 10^3−10^5 times that of the original concentration. Similar results have been obtained by studies of methylene blue.[31] The freeze concentration in the order of 10^2−10^3 was found for amino acids;[63] a 10^1−10^2 times increase in concentration was calculated for various salts in seawater.[64] The degree of freeze concentration depends primarily on several factors—temperature, solubility, and initial concentration. Higher solubility enhances the freeze concentration, as do decreasing temperature and initial concentration. The results of the mentioned studies differ mainly because the initial concentrations vary, and the initial concentration of the solutions of amino acids ($c \approx 20$−300 mg/mL)[63] was larger than the initial MB concentration, which was studied for the range of low concentrations ($c \approx 10^{-3}$ to 10^{-6} M).

The effect of initial concentration can also be seen in the log−log plot in Figure 8A. It shows that the logarithm of concentration factor scales linearly with the negative logarithm of acid concentration up to roughly a concentration of 20 mM. However, if all the data are fitted with a line (Figure S13), a clear trend in the residuals is visible on the whole concentration interval: It resembles a parabolic function, suggesting that the line predicts a lower concentration factor for high and low initial HCl concentrations. Therefore, only concentrations up to $-\log(c) = 1.69$ were fitted with a line (Figure 8A) and residuals from the fit show no significant trend up to this concentration. However, the underlying trend of a slight decline of the logarithm of concentration factor with increasing negative log of concentration (thus decreasing concentration) is clearly visible (Figure 8B).

This deviation from the linear trend can be attributed to two factors—first is the presence of HCl-quenched phases (Figure 5A), which is also visible from the thermograms (Figures 3 and 4 and Figures S4 and S5). The phases that are not fully saturated with HCl show acidity lower than that of the eutectic composition. The indicator should be distributed between all these phases; thus, an "average" is obtained from each measurement. It would make sense that with an increasing portion of the quenched undersaturated phases, the acidity decreases (based on the trend in Figure 5A). The second effect that can take place is the incorporation of chloride ions into the ice, which would decrease the concentration of chlorides in FCS. The incorporation of chlorides into the ice would be countered by protons. This very process decreases the acidity of the FCS probed by the indicator, as was observed for NaCl[15,16] and other salts.[17]

It has been suggested that ice is able to accommodate chloride ions up to a limiting concentration of 2×10^{-4} M, depending on the concentration near the ice interface.[65] Lower concentrations of NaCl near the ice−solution interface significantly decrease the number of incorporated chlorides. Their maximum concentration was reported to be close to 3×10^{-4} M,[66] and even higher values were estimated from the molecular dynamic simulations.[67]

It is obvious that the highest level of incorporation should occur in the 1 M sample. However, the concentration of incorporated chlorides and protons would be at most 3×10^{-4} M, which is negligible compared to the concentration of HCl in the FCS. With a lower initial concentration, the concentration of incorporated protons would decrease. That is why we can observe the behavior of freeze-concentrated HCl solutions even at a concentration of 10^{-5} M HCl. Nonetheless, this second effect would work in tandem with the first one, lowering the acidity further, where the two effects are not separable from the present data.

CONCLUSIONS

Differential scanning calorimetry was used to investigate the behavior of frozen HCl solutions during thawing for concentrations of 1 M, 100 mM, and 10 mM. The solutions studied exhibit a glass-to-liquid transition at approximately −138 °C and a cold crystallization exotherm at −110 °C. This means that in the temperature range of −138 to −110 °C, there is a viscous liquid in the ice matrix, which is unable to crystallize. At −110 °C, cold crystallization produces mainly $HCl{\cdot}6H_2O$ in an exothermic process. Melting of ice/hydrochloric acid hexahydrate occurs at −75 °C and is observed as a significant endotherm in the thermogram. Samples with 100

https://doi.org/10.1021/acs.jpcc.4c04540
J. Phys. Chem. C 2024, 128, 17674−17685

and 10 mM concentrations show a similar type of phase behavior, with additional small thermal signatures in the range of −50 and −30 °C, indicating the presence of quenched HCl phases that are lower in concentration compared to the eutectic ($HCl·6H_2O$) for which cooling in liquid nitrogen is required. The state/phase transitions observed calorimetrically induce the acidity changes determined by in situ acid−base indicator UV−vis spectrophotometry. Cold crystallization of $HCl·6H_2O$ causes a decrease in acidity, whereas melting of the ice/hexahydrate causes an increase in acidity. The magnitude of this effect depends on the initial solution concentration. Furthermore, the results show that samples of higher concentrations (1 M−20 mM) freeze-concentrate approximately to the eutectic concentrations (from about 7.62 to 6.61 M), whereas samples of lower initial concentration freeze-concentrate to much lower values. However, the sample with the lowest initial concentration (c = 5 μM HCl) still freeze-concentrates by a factor of about 250,000. The results presented here are consistent with the previously elucidated freeze-concentration effects with other solutes.[31]

■ ASSOCIATED CONTENT

Supporting Information

The Supporting Information is available free of charge at https://pubs.acs.org/doi/10.1021/acs.jpcc.4c04540.

Spectra taken during the titration of BCP and CPR; pure forms of said indicators are elucidated from the titration spectra; heating thermograms of HCl solutions and their derivatives; spectra of BCP frozen in the HCl solutions and their respective acidities; fit of all acidity values at the temperatures of approximately −150 and −115 °C; schematic depiction of the thermal behavior of HCl during freezing and thawing; enthalpy values obtained by trapezoid integration of the respective thermograms of HCl solutions of various concentrations; acidity of the frozen HCl samples depending on the temperature of the sample; Hammett acidities at temperatures of −150 and −115 °C; and HCl concentration to Hammett acidity and vice versa (PDF)

■ AUTHOR INFORMATION

Corresponding Author

Dominik Heger − *Department of Chemistry, Faculty of Science, Masaryk University, Brno 625 00, Czech Republic;* orcid.org/0000-0002-6881-8699; Phone: +420 549 49 3322; Email: hegerd@chemi.muni.cz

Authors

Radim Štůsek − *Department of Chemistry, Faculty of Science, Masaryk University, Brno 625 00, Czech Republic*

Lukáš Veselý − *Department of Chemistry, Faculty of Science, Masaryk University, Brno 625 00, Czech Republic;* orcid.org/0000-0003-2179-9395

Markéta Melicharová − *Department of Chemistry, Faculty of Science, Masaryk University, Brno 625 00, Czech Republic*

Jan Zezula − *Department of Chemistry, Faculty of Science, Masaryk University, Brno 625 00, Czech Republic*

Johannes Giebelmann − *Institute of Physical Chemistry, University of Innsbruck, Innsbruck 6020, Austria;* orcid.org/0000-0003-4529-5124

Thomas Loerting − *Institute of Physical Chemistry, University of Innsbruck, Innsbruck 6020, Austria;* orcid.org/0000-0001-6694-3843

Complete contact information is available at: https://pubs.acs.org/10.1021/acs.jpcc.4c04540

Author Contributions

Radim Štusek: conceptualization, software, investigation, visualization, writing−original draft preparation, and funding acquisition. Lukáš Veselý: conceptualization, writing—reviewing and editing, and validation. Markéta Melicharová: data curation. Jan Zezula: data curation. Thomas Loerting: writing—reviewing and editing. Johannes Giebelmann: writing—reviewing and editing, methodology. Dominik Heger: conceptualization, supervision, resources, writing—reviewing and editing.

Notes

The authors declare no competing financial interest.

■ ACKNOWLEDGMENTS

The authors would like to acknowledge the support of the Masaryk University grant agency (GAMU) through the project MUNI/C/0104/2023 and support of CEEPUS grant M-SI-1312-2223-170532.

■ REFERENCES

(1) Horsford, E. N. I. On the Source of Free Hydrochloric Acid in the Gastric Juice. *Proc. R. Soc. London* **1869**, *17*, 391−395.

(2) Nara, S.; et al. Validation of Smiles Hcl Profiles over a Wide Range from the Stratosphere to the Lower Thermosphere. *Atmos. Meas. Technol.* **2020**, *13*, 6837−6852.

(3) Kama, M.; et al. Depletion of Chlorine into Hcl Ice in a Protostellar Core. *A&A* **2015**, *574*, A107.

(4) Mani, D.; et al. Acid Solvation Versus Dissociation at "Stardust Conditions": Reaction Sequence Matters. *Sci. Adv.* **2019**, *5*, No. eaav8179.

(5) Dhooghe, F.; et al. Halogens as Tracers of Protosolar Nebula Material in Comet 67p/Churyumov−Gerasimenko. *Mon. Not. R. Astron. Soc.* **2017**, *472*, 1336−1345.

(6) Luginin, M.; Trokhimovskiy, A.; Taysum, B.; Fedorova, A. A.; Korablev, O.; Olsen, K. S.; Montmessin, F.; Lefèvre, F. Evidence of Rapid Hydrogen Chloride Uptake on Water Ice in the Atmosphere of Mars. *Icarus* **2024**, *411*, No. 115960.

(7) Krasnopolsky, V. A. Photochemistry of Hcl in the Martian Atmosphere. *Icarus* **2022**, *374*, No. 114807.

(8) McNeill, V. F.; Loerting, T.; Geiger, F. M.; Trout, B. L.; Molina, M. J. Hydrogen Chloride-Induced Surface Disordering on Ice. *Proc. Natl. Acad. Sci. U. S. A.* **2006**, *103*, 9422−9427.

(9) Solomon, S.; Garcia, R. R.; Rowland, F. S.; Wuebbles, D. J. On the Depletion of Antarctic Ozone. *Nature* **1986**, *321*, 755−758.

(10) Molina, M. J.; Tso, T.-L.; Molina, L. T.; Wang, F. C.-Y. Antarctic Stratospheric Chemistry of Chlorine Nitrate, Hydrogen Chloride, and Ice: Release of Active Chlorine. *Science* **1987**, *238*, 1253−1257.

(11) Pawar, P. V.; et al. Chloride (HCl/Cl-) dominates inorganic aerosol formation from ammonia in the Indo-Gangetic Plain during winter: modeling and comparison with observations. *Atmos. Chem. Phys.* **2023**, *23*, 41−59.

(12) Semeniuk, K.; Dastoor, A. Current State of Atmospheric Aerosol Thermodynamics and Mass Transfer Modeling: A Review. *Atmosphere* **2020**, *11*, 156.

(13) Thibert, E.; Dominé, F. Thermodynamics and Kinetics of the Solid Solution of Hcl in Ice. *J. Phys. Chem. B* **1997**, *101*, 3554−3565.

(14) Workman, E. J.; Reynolds, S. E. Electrical Phenomena Occurring During the Freezing of Dilute Aqueous Solutions and

Their Possible Relationship to Thunderstorm Electricity. *Phys. Rev.* **1950**, *78*, 254−259.
(15) Imrichová, K.; Veselý, L.; Gasser, T. M.; Loerting, T.; Neděla, V.; Heger, D. Vitrification and Increase of Basicity in between Ice Ih Crystals in Rapidly Frozen Dilute Nacl Aqueous Solutions. *J. Chem. Phys.* **2019**, *151*, No. 014503.
(16) Heger, D.; Klánová, J.; Klán, P. Enhanced Protonation of Cresol Red in Acidic Aqueous Solutions Caused by Freezing. *J. Phys. Chem. B* **2006**, *110*, 1277−1287.
(17) Krausková, Ĺ.; Procházková, J.; Klašková, M.; Filipová, L.; Chaloupková, R.; Malý, S.; Damborský, J.; Heger, D. Suppression of Protein Inactivation During Freezing by Minimizing Ph Changes Using Ionic Cryoprotectants. *Int. J. Pharm.* **2016**, *509*, 41−49.
(18) Abbatt, J. P. D.; Beyer, K. D.; Fucaloro, A. F.; McMahon, J. R.; Wooldridge, P. J.; Zhang, R.; Molina, M. J. Interaction of Hcl Vapor with Water-Ice: Implications for the Stratosphere. *Journal of Geophysical Research: Atmospheres* **1992**, *97*, 15819−15826.
(19) Bogdan, A.; Molina, M. J.; Kulmala, M.; MacKenzie, A. R.; Laaksonen, A. Study of Finely Divided Aqueous Systems as an Aid to Understanding the Formation Mechanism of Polar Stratospheric Clouds: Case of Hno3/H2o and H2so4/H2o Systems. *J. Geophys. Res.: Atmos.* **2003**, *108*, 4302.
(20) Bogdan, A.; Loerting, T. Phase Separation During Freezing Upon Warming of Aqueous Solutions. *J. Chem. Phys.* **2014**, *141*, 18C533.
(21) Hammer, C. U. Acidity of Polar Ice Cores in Relation to Absolute Dating, Past Volcanism, and Radio−Echoes. *Journal of Glaciology* **1980**, *25*, 359−372.
(22) Stillman, D. E.; MacGregor, J. A.; Grimm, R. E. The Role of Acids in Electrical Conduction through Ice. *Journal of Geophysical Research: Earth Surface* **2013**, *118*, 1−16.
(23) Köster, K.; Fuentes-Landete, V.; Raidt, A.; Seidl, M.; Gainaru, C.; Loerting, T.; Böhmer, R. Dynamics Enhanced by Hcl Doping Triggers 60% Pauling Entropy Release at the Ice Xii−Xiv Transition. *Nat. Commun.* **2015**, *6*, 7349.
(24) Köster, K.; Raidt, A.; Fuentes Landete, V.; Gainaru, C.; Loerting, T.; Böhmer, R. Doping-Enhanced Dipolar Dynamics in Ice V as a Precursor of Hydrogen Ordering in Ice Xiii. *Phys. Rev. B* **2016**, *94*, No. 184306.
(25) Bartels-Rausch, T.; et al. A Review of Air−Ice Chemical and Physical Interactions (Aici): Liquids, Quasi-Liquids, and Solids in Snow. *Atmos. Chem. Phys.* **2014**, *14*, 1587−1633.
(26) Ondrušková, G.; Krausko, J.; Stern, J. N.; Hauptmann, A.; Loerting, T.; Heger, D. Distinct Speciation of Naphthalene Vapor Deposited on Ice Surfaces at 253 or 77 K: Formation of Submicrometer-Sized Crystals or an Amorphous Layer. *J. Phys. Chem. C* **2018**, *122*, 11945−11953.
(27) Krausko, J.; Malongwe, J. K. E.; Bičanová, G.; Klán, P.; Nachtigallová, D.; Heger, D. Spectroscopic Properties of Naphthalene on the Surface of Ice Grains Revisited: A Combined Experimental−Computational Approach. *J. Phys. Chem. A* **2015**, *119*, 8565−8578.
(28) Kania, R.; Malongwe, J. K. E.; Nachtigallová, D.; Krausko, J.; Gladich, I.; Roeselová, M.; Heger, D.; Klán, P. Spectroscopic Properties of Benzene at the Air−Ice Interface: A Combined Experimental−Computational Approach. *J. Phys. Chem. A* **2014**, *118*, 7535−7547.
(29) Krausko, J.; Runštuk, J.; Neděla, V.; Klán, P.; Heger, D. Observation of a Brine Layer on an Ice Surface with an Environmental Scanning Electron Microscope at Higher Pressures and Temperatures. *Langmuir* **2014**, *30*, 5441−5447.
(30) Vetráková, Ľ.; Neděla, V.; Runštuk, J.; Heger, D. The Morphology of Ice and Liquid Brine in an Environmental Scanning Electron Microscope: A Study of the Freezing Methods. *Cryosphere* **2019**, *13*, 2385−2405.
(31) Heger, D.; Jirkovský, J.; Klán, P. Aggregation of Methylene Blue in Frozen Aqueous Solutions Studied by Absorption Spectroscopy. *J. Phys. Chem. A* **2005**, *109*, 6702−6709.
(32) Mulvaney, R.; Wolff, E. W.; Oates, K. Sulphuric Acid at Grain Boundaries in Antarctic Ice. *Nature* **1988**, *331*, 247−249.
(33) Fukazawa, H.; Sugiyama, K.; Mae, S.; Narita, H.; Hondoh, T. Acid Ions at Triple Junction of Antarctic Ice Observed by Raman Scattering. *Geophys. Res. Lett.* **1998**, *25*, 2845−2848.
(34) Wolff, E. W.; Mulvaney, R.; Oates, K. The Location of Impurities in Antarctic Ice. *Annals of Glaciology* **1988**, *11*, 194−197.
(35) Hammer, C. U.; Clausen, H.; Dansgaard, W.; Neftel, A.; Kristinsdottir, P.; Johnson, E. Continuous Impurity Analysis Along the Dye 3 Deep Core. *Greenland ice core: geophysics, geochemistry, and the environment* **1985**, *33*, 90−94.
(36) Veselý, L.; Závacká, K.; Štůsek, R.; Olbert, M.; Neděla, V.; Shalaev, E.; Heger, D. Impact of Secondary Ice in a Frozen Nacl Freeze-Concentrated Solution on the Extent of Methylene Blue Aggregation. *Int. J. Pharm.* **2024**, *650*, No. 123691.
(37) Hauptmann, A.; Hoelzl, G.; Loerting, T. Distribution of Protein Content and Number of Aggregates in Monoclonal Antibody Formulation after Large-Scale Freezing. *AAPS PharmSciTech* **2019**, *20*, 72.
(38) Bogdan, A.; Molina, M. J.; Tenhu, H.; Loerting, T. Multiple Glass Transitions and Freezing Events of Aqueous Citric Acid. *J. Phys. Chem. A* **2015**, *119*, 4515−4523.
(39) Najim, A.; Krishnan, S. Experimental Study on Progressive Freeze-Concentration Based Desalination Employing a Rectangular Channel Crystallizer. *Environmental Science: Water Research & Technology* **2023**, *9*, 850−860.
(40) Prestes, A. A.; Helm, C. V.; Esmerino, E. A.; Silva, R.; da Cruz, A. G.; Prudencio, E. S. Freeze Concentration Techniques as Alternative Methods to Thermal Processing in Dairy Manufacturing: A Review. *J. Food Sci.* **2022**, *87*, 488−502.
(41) Ruiz-Rodríguez, A.; Durán-Guerrero, E.; Natera, R.; Palma, M.; Barroso, C. G. Influence of Two Different Cryoextraction Procedures on the Quality of Wine Produced from Muscat Grapes. *Foods* **2020**, *9*, 1529.
(42) Qu, H.; Arai, Y.; Harada, M.; Okada, T. Freeze Enrichment Protocol Based on Voltammetric Probing of Liquid-Phase Growth in Frozen Aqueous Electrolyte Solutions. *Anal. Chem.* **2015**, *87*, 4314−4320.
(43) Shalaev, E. Y.; Franks, F.; Echlin, P. Crystalline and Amorphous Phases in the Ternary System Water− Sucrose− Sodium Chloride. *J. Phys. Chem.* **1996**, *100*, 1144−1152.
(44) Shalaev, E. Y.; Franks, F. Changes in the Physical State of Model Mixtures During Freezing and Drying: Impact on Product Quality. *Cryobiology* **1996**, *33*, 14−26.
(45) Hauptmann, A.; Podgoršek, K.; Kuzman, D.; Srčič, S.; Hoelzl, G.; Loerting, T. Impact of Buffer, Protein Concentration and Sucrose Addition on the Aggregation and Particle Formation During Freezing and Thawing. *Pharm. Res.* **2018**, *35*, 101.
(46) Beyer, K. D.; Hansen, A. R. Phase Diagram of the Nitric Acid/Water System: Implications for Polar Stratospheric Clouds. *J. Phys. Chem. A* **2002**, *106*, 10275−10284.
(47) Beyer, K. D.; Hansen, A. R.; Poston, M. The Search for Sulfuric Acid Octahydrate: Experimental Evidence. *J. Phys. Chem. A* **2003**, *107*, 2025−2032.
(48) Marion, G. M. A Molal-Based Model for Strong Acid Chemistry at Low Temperatures (<200 to 298 K). *Geochim. Cosmochim. Acta* **2002**, *66*, 2499−2516.
(49) Rupert, F. F. A Study of the System Hydrogen Chloride and Water. *J. Am. Chem. Soc.* **1909**, *31*, 851−866.
(50) Pickering, S. U. Lxxi.—a Study of the Properties of Some Strong Solutions. *Journal of the Chemical Society, Transactions* **1893**, *63*, 998−1027.
(51) Vetráková, Ľ.; Vykoukal, V.; Heger, D. Comparing the Acidities of Aqueous, Frozen, and Freeze-Dried Phosphate Buffers: Is There a "Ph Memory" Effect? *Int. J. Pharm.* **2017**, *530*, 316−325.
(52) Susrisweta, B.; Veselý, L.; Štůsek, R.; Hauptmann, A.; Loerting, T.; Heger, D. Investigating Freezing-Induced Acidity Changes in Citrate Buffers. *Int. J. Pharm.* **2023**, *643*, No. 123211.
(53) Veselý, L.; Susrisweta, B.; Heger, D. Making Good's Buffers Good for Freezing: The Acidity Changes and Their Elimination Via Mixing with Sodium Phosphate. *Int. J. Pharm.* **2021**, *593*, No. 120128.

https://doi.org/10.1021/acs.jpcc.4c04540
J. Phys. Chem. C 2024, 128, 17674−17685

(54) Ondrušková, G.; Veselý, L. s.; Zezula, J.; Bachler, J.; Loerting, T.; Heger, D. Using Excimeric Fluorescence to Study How the Cooling Rate Determines the Behavior of Naphthalenes in Freeze-Concentrated Solutions: Vitrification and Crystallization. *J. Phys. Chem. B* **2020**, *124*, 10556−10566.
(55) Yao, W.; Byrne, R. H. Spectrophotometric Determination of Freshwater Ph Using Bromocresol Purple and Phenol Red. *Environ. Sci. Technol.* **2001**, *35*, 1197−1201.
(56) Christian, G. D.; Rosenthal, D. The Effects of Salts on Titrations. *CRC Crit. Rev. Anal. Chem.* **1975**, *5*, 119−163.
(57) Paul, M. A.; Long, F. A. H0 and Related Indicator Acidity Function. *Chem. Rev.* **1957**, *57*, 1−45.
(58) Meloun, M.; Kotrly, S. Multiparametric Curve Fitting 0.2. Determination of Thermodynamic Dissociation-Constants and Parameters of Extended Debye-Huckel Expression - Application for Some Sulfonaphthalein Indicators. *COLLECTION OF CZECHOSLOVAK CHEMICAL COMMUNICATIONS* **1977**, *42*, 2115−2125.
(59) Kresge, A. J.; Chen, H. J.; Capen, G. L.; Powell, M. F. Extrapolation from Concentrated to Dilute Aqueous Acids. *Can. J. Chem.* **1983**, *61*, 249−256.
(60) Loerting, T.; Salzmann, C.; Kohl, I.; Mayer, E.; Hallbrucker, A. A Second Distinct Structural "State" of High-Density Amorphous Ice at 77 K and 1 bar. *Phys. Chem. Chem. Phys.* **2001**, *3*, 5355−5357.
(61) Gasser, T. M.; Thoeny, A. V.; Fortes, A. D.; Loerting, T. Configurational Entropy of Ice Xix and Its Isotope Effect. *Sci. Rep.* **2024**, *14*, 10517.
(62) Hofer, K.; Astl, G.; Mayer, E.; Johari, G. Vitrified Dilute Aqueous Solutions. 4. Effects of Electrolytes and Polyhydric Alcohols on the Glass Transition Features of Hyperquenched Aqueous Solutions. *J. Phys. Chem.* **1991**, *95*, 10777−10781.
(63) Dong, J.; Hubel, A.; Bischof, J. C.; Aksan, A. Freezing-Induced Phase Separation and Spatial Microheterogeneity in Protein Solutions. *J. Phys. Chem. B* **2009**, *113*, 10081−10087.
(64) Marion, G. M.; Farren, R. E.; Komrowski, A. J. Alternative Pathways for Seawater Freezing. *Cold Regions Science and Technology* **1999**, *29*, 259−266.
(65) Seidensticker, R. G. Partitioning of Hcl in the Water-Ice System. *J. Chem. Phys.* **1972**, *56*, 2853−2857.
(66) Moore, J. C.; Reid, A. P.; Kipfstuhl, J. Microstructure and Electrical Properties of Marine Ice and Its Relationship to Meteoric Ice and Sea Ice. *Journal of Geophysical Research: Oceans* **1994**, *99*, 5171−5180.
(67) Conde, M. M.; Rovere, M.; Gallo, P. Spontaneous Nacl-Doped Ice at Seawater Conditions: Focus on the Mechanisms of Ion Inclusion. *Phys. Chem. Chem. Phys.* **2017**, *19*, 9566−9574.

https://doi.org/10.1021/acs.jpcc.4c04540
J. Phys. Chem. C 2024, 128, 17674−17685